CAV2009 - Paper No.

SHALLOW ANGLE WATER ENTRY OF BALLISTIC PROJECTILES

Tadd T. Truscott *
Department of Mechanical Engineering
Massachusetts Institute of Technology
Cambridge, MA 02139
Email: truscott@mit.edu

David N. Beal
Naval Underwater Warfare Center
Code 8233
Newport, Rhode Island 02841-1708
Email: david.beal@navy.mil

Alexandra H. Techet
Department of Mechanical Engineering
Massachusetts Institute of Technology
Cambridge, MA 02139
Email: ahtechet@mit.edu

ABSTRACT

The water-entry of ballistic projectiles is investigated using high-speed digital imaging to capture the subsurface cavity dynamics. Specially designed 0.22 caliber projectiles are fired into water at shallow angles to the free surface ($5°$ to $15°$) at Mach numbers between 0.3 and 1.0. Redesigned projectile tip geometries allowed projectiles to successfully enter the water and travel large distances underwater, due to the subsurface vapor-cavity that forms after impact, dramatically decreasing drag on the projectile. Projectile dynamics, critical entry angle and cavity formation are discussed for various bullet geometries, and results show that successful water-entry is a function of tip shape and length-to-diameter ratio. The data conclusively show that bullets with lower length-to-diameter ratios tumble inside the vapor cavity, while higher length-to-diameter ratios can lean against the cavity walls inducing a planing force pushing them back inside the cavity and mitigating the tumbling behavior. Experimental cavity observations of vapor-cavity formation is compared to a modified version of Logvinovich's [1] theoretical model, which includes an updated formulation of the model and an angle of attack correction. Despite the unsteady nature of this problem, this improved steady state model fits well with experimental data and serves as an accurate design tool for naval engineers.

_____

*Address all correspondence to this author.

INTRODUCTION

The designs for bullet geometry, velocities, and spin rates vary considerably for projectiles fired in the air versus the water. Typically projectiles launched from air into water are fired at high angles ($90°$) to the free surface [2]. At shallow angles ($5-15°$) standard ballistic projectiles do not enter the water, instead they ricochet off the surface or break into many pieces. Projectiles designed to enter the water at shallow angles are designed with blunt tips and large length to diameter ratios, which create a vaporous supercavity that originates at the tip of the bullet upon impact with the free surface. The vapor cavity greatly reduces the drag of the projectile by diminishing its frontal area and viscous interaction. These projectiles ride inside of the cavity using the sidewall as a stabilization mechanism [3].

Several experimental studies have looked at vertical air-water impact of high-speed projectiles [4, 5, 6]. One of the most complete published study to date was performed by [3], in which a fully developed underwater cavity is formed by firing projectiles underwater, avoiding the free surface interaction and thus creating optimal conditions for determining the mechanisms of underwater stability as well as nearly steady state vapor-cavity size estimates. Several full-scale, shallow-angle, air-to-water studies have been performed by different researcher groups but none have been published to date. Several theoretical cavity models have been developed as well. [1] and [7] have developed analytical models for cavity formation and cavity oscillations based partially on empirical data and mostly on control volume analysis; while others such as [8] have focused more on the projectile stability. [9] wrote an entire volume of work on the
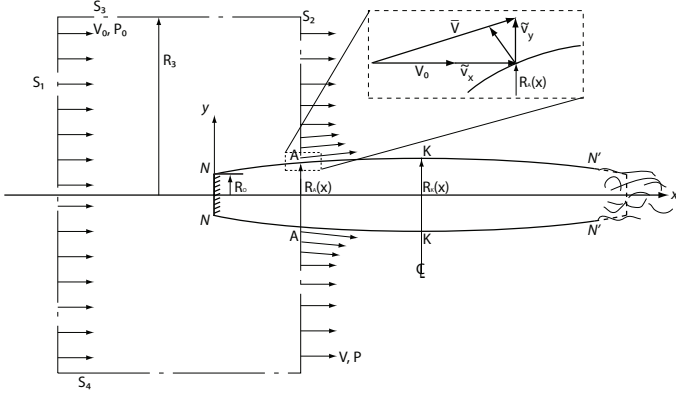
Figure 1. Two dimensional sketch of disc NN in a velocity (V_o) and pressure (P_o) field, used in the axisymmetric control volume approach to determine the cavity shape.

subject of hydroballistics, which includes a excellent summary of both quantitative and qualitative experimental data taken by Albert May [4, 10, 11]. More recently [12] used a numerical simulation employing preconditioning to estimate the cavity shape, temperature, shock formation, and pressure inside and outside of the cavity of bullet water entry. [9] comments on the need for experiments that include oblique entry from air to water.

We present experimental data for three particular bullet shapes impacting the free surface at shallow angles fired at roughly the same muzzle velocity ($V_m = 380$ m/s) for which three distinctly different cavities form. The bullet position and cavity shapes are determined through image processing. Force and moment data are indirectly measured by fitting splines to the position data to determine the deceleration of the bullets. Additionally, we re-formulate the model originally presented in [1] improving the empirical fit and include a small correction for yaw and pitch of the projectile inside of the cavity. The model was then used to design the modified bullet presented, which travels at much higher velocities than the other projectiles.

THEORETICAL MODEL

Theoretical modeling is useful in predicting cavity geometry and designing projectile shapes. With improved ballistic design, the ability for these projectiles to enter the water and maintain significant speed can be enhanced. Logvinovich [1] derived a classical model for an axisymmetric cavity behind a supercavitating bullet by modeling the bullet as a disc transverse to an oncoming flow. His model used an empirical fit to the front section of the cavity and an analytical solution aft of the fit. We revisit the Logvinovich model and reformulate the fitting parameters to produce cavities that are continuous for all values downstream of the disc (x).

The axisymmetric analytical model is derived assuming that

a vapor cavity is formed by a disc of radius R_o in a uniform ideal flow of speed V_o. Figure 1 shows a two dimensional sketch of the disc in the flow field and the associated cavity. The cavity is formed at the leading edge of the disc NN and the downstream section of the cavity $N'N'$ far from the disc; the bubbly foamy flow behind the cavity is neglected in this model. For this approach to work, cavitation in the wake of the disc must be ensured. Thus the fluid pressure must be less than the fluid vapor pressure. The cavitation number, used to characterize the potential of the fluid to cavitate, is the ratio of the difference between the fluid pressure (P) and the vapor pressure (P_v) to the kinetic energy per volume ($\frac{1}{2}\rho V^2$),

$$\sigma = \frac{P - P_v}{\frac{1}{2}\rho V^2} \tag{1}$$

where *large* cavities typically form when $\sigma < 0.1$ [1].

The cavity is broken up into two parts: the *leading* section, which extends from the tip of the disc (NN) aft to a point approximately two to five disc radii behind the tip x_1; and the *trailing* section $x > x_1$. x_1 is the point at which the formula describing the cavity for both the leading and trailing sections yield equal values for the cavity radius $R_1 = R(x_1)$. Following [1], the radius of the *leading* part of the cavity can be expressed approximately from empirical evidence as

$$R(x) = R_0 \left(1 + 3\frac{x}{R_0}\right)^{1/3}; \tag{2}$$

this empirical model is valid only for cavitation numbers below $\sigma < 0.1$ and $x/R_0 < 5$.

The radius of the *trailing* part of the cavity is determined by applying the momentum theorem around a cylindrical control volume (figure 1); a full derivation of this model can be found in [1] and also [13]. The final result from [1] for the cavity radius as a function of distance behind the disc is given as

$$R(x) = R_k \sqrt{1 - \left(1 - \frac{R_1^2}{R_k^2}\right)\left|\left(1 - \frac{x}{x_k}\right)\right|^{1/\chi}}, \tag{3}$$

where $\chi = 0.85$ is a correction factor, R_k is the maximum radius of the cavity at x_k, the distance downstream from the disc to KK. The control volume analysis from [1] is only valid up to the maximum radius R_k, which is sufficient for our purposes since the bullets used in this study fit well within this limit, but could be an issue for larger ballistic missiles.

Logvinovich calculates the location of x_1 using two additional correction factors. In his formulation, Logvinovich only requires that $R(x_1)$ be equal for both equation 2 and 3, but does
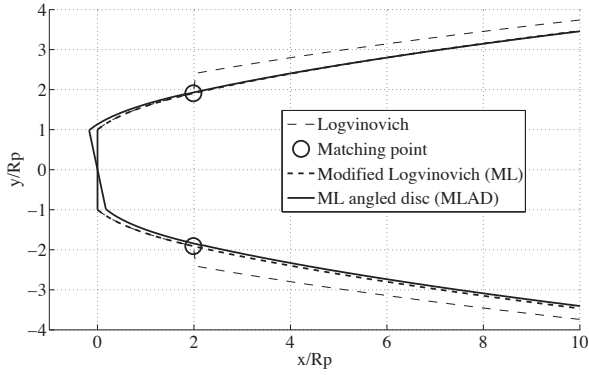
Figure 2. Cavity outlines for three different theoretical approaches as indicated in legend. (○) represents the matching point location for all three models as the transition point from the empirical model at the tip to the analytic model.
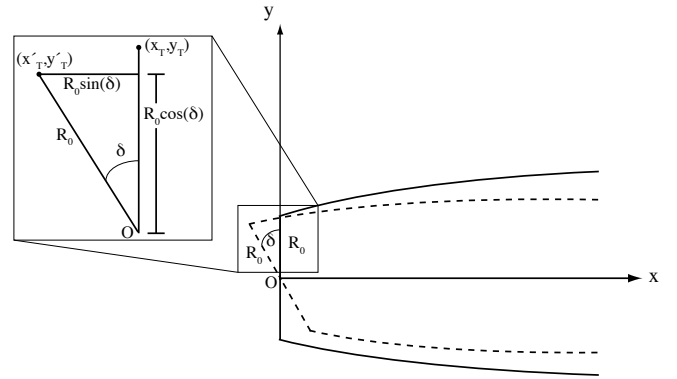

Figure 3. Sketch of the cavity near the tip of the disc illustrating how the cavity size is determined when the disc is at an angle (δ) to the incoming flow field. The inset shows the disc rotated by an angle δ compared to the vertical and shows how the projected area facing the flow V_o is reduced.

not require that the slopes of the cavity radius dR_1/dx be equal. Logvinovich recognizes this shortcoming, but reasons that so long as the matching point is $x < 5R_0$ his methodology is acceptable. However, in the experiments performed in our study, the matching point found using the Logvinovich model is much further downstream at $x = 11R_0$, well beyond the point at which the empirical results for the *leading* section breaks down. Thus, we require that the slope of the cavity radius match at x_1 along with the cavity radius, and set the matching point to be at $x_1 = 2R_0$, effectively eliminating the two additional correction factors used in [1]. The slope of R_1 is derived from equation 2 as

$$\frac{dR_1}{dx} = V_0 \left(1 + \frac{3x_1}{R_0} \right)^{-\frac{2}{3}}, \tag{4}$$

Logvinovich also defines the maximum cavity radius for the steady state as $R_k = R_0\sqrt{C_{x0}(1+\sigma)/\sigma}$, where the drag coefficient for a disc cavitator in a flow field is measured as $C_{x0} = 0.82$, leaving only one remaining variable to determine x_k. Truscott [13] derives this distance from the disc to the maximum cavity radius as

$$x_k = \frac{R_k^2 - R_1^2}{2\chi R_1} \left(\frac{1}{\partial R_1 / \partial x} \right), \tag{5}$$

which is only a function of the initial disc radius, the empirical drag coefficient acting on the disc, the cavitation number and the empirical constant χ. This method yields cavities that are continuous for all values of x regardless of the empirical model used near the tip.

A comparison of the original formulation of Logvinovich and the modified formulation presented here is shown in figure 2. In order to compare these models with an experimental data set, we specify the disc radius R_0 to correspond with one of the ballistic cases we present in the Experimental Results section (case 7). For this case, the Logvinovich model required that $x_1 = 11R_0$, at which the empirical formula for $R(x)$ is no longer valid. Therefore we fix the matching point for the Logvinovich model to $x_1 = 2R_0$, chosen such that we can compare directly with our modified theory. Figure 2 reveals that the Logvinovich model predicts a discontinuity in cavity radius near x_1, due to being forced to match at $x_1 = 2R_0$ instead of $x_1 = 11R_0$, making the cavity larger than it should be down stream of the matching point.

During experiments it was noted that the projectiles have a tendency to pitch and yaw inside the cavity. One way of improving the axisymmetric model presented here is to capture this motion at least in pitch, for now neglecting the out-of-plane yaw motion, which could not accurately be determined from experimental data. First, the projectile tip is represented by a disc with an angle of δ traveling in the direction of V_0 (figure 3). Next we assume that for small pitch angles ($\delta < 15°$), the angled disc can be represented effectively as a disc with a reduced radius $R' = R_0 cos(\delta)$. The cavity is then modeled using the reduced radius disc. The upper and lower cavity outlines are then translated to connect with the location of the angled disc edges. The upper cavity translates by $[x'_T = x - R_o sin(\delta), y'_T = R(x) - R_o cos(\delta)]$, and the lower cavity translates to $[x'_B = x + R sin(\delta), y'_B = R(x) - R cos(\delta)]$. The results from the angled disc modification are compared to the other two modeling methods in figure 2. This angle adjustment is included in comparisons of the theoretical model with experimental data in following sections.

3

EXPERIMENTAL DETAILS

Laboratory scale experiments were performed to elucidate the dynamics of ballistic-type projectiles fired at high velocity into a tank of water at shallow entry angles to the free surface. Standard and modified 0.22 caliber ballistic projectiles were fired into a custom built bullet-proof tank at the MIT Rifle Range. High quality, high-speed imaging combined with precise timing and remote triggering were critical for the success of this experimental investigation. Details of the experimental setup are presented herein.

Experimental Facility

A bullet-proof tank (1.8 m × 0.6 m × 0.6 m) was constructed from 1.9 cm thick clear Lexan$^{®}$ walls. The tank was filled to a depth of 0.45 m, and the end wall near the entry site was lowered to allow the projectiles to be shot at very shallow angles at the free surface (figure 4). The far end of the tank was protected from bullet impacts by two large 1 cm thick steel plates, one at the bottom of the tank and the other inclined at an angle to deflect bullets down and into the water in case of surface ricochet. The tank was reinforced externally by 80/20$^{®}$ Inc. aluminum extrusions. The experimental was performed at the MIT Rifle Range facility.
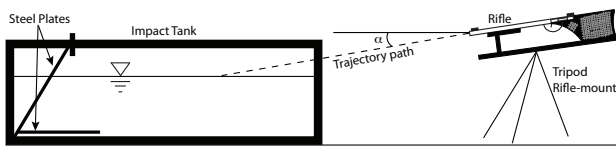
Figure 4. Gun and impact tank set up viewed from side. The gun is mounted on a tripod and aimed at a shallow angle (α) to the free surface inside the tank. The trajectory appears to pass through the front side of the tank (right side in image), but in reality the front wall is shorter to accommodate for this. Two steel plates help decrease ricochet and impact with the back of the tank (left side).

The projectiles tested included standard 0.22 caliber bullets as well as custom bullets, which were reloaded into standard 0.22 caliber bullet casings as shown in figure 5. Most standard 0.22 caliber bullets are designed to split apart or deform after impact with a target, which typically ensures that the kinetic energy of the bullet is converted into damage of the target. During water entry, the shallow angled impact of a standard 0.22 caliber bullet does not cause large deformations, but instead causes a large pitching or yawing moment, which induces tumbling and erratic behavior down range (see Experimental Results). To mitigate the effect of deformation and tumbling, custom bullets were designed with high length to diameter ratios, special tip shapes, and
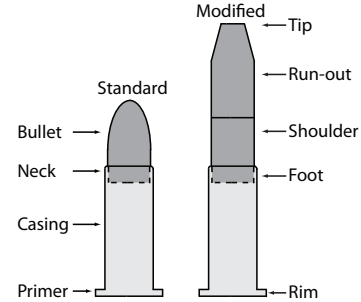
Figure 5. Drawing of a standard and modified 0.22 caliber bullet and relevant nomenclature (not to scale).

materials strong enough to resist deformation at these speeds (below the sound limit in air). A schematic of a generalized modified bullet geometry compared to a standard 0.22 is shown in Figure 5.

Custom bullet designs were manufactured using one of three materials: bronze, steel, or aluminum. The material, length to diameter ratio and tip design was altered for each bullet, but the overall weight of the bullet kept constant for all bullet shapes. The weight was fixed to be the same as that of a typical 0.22 caliber bullet, such that the 0.22 caliber powder and primer would have a similar accelerating affect on the prototype bullets as on a standard 0.22 caliber bullet. The maximum weight of a 0.22 caliber bullet is 40 grains (2.59 grams) and the maximum diameter is 0.22 in (5.5 mm). Material densities and projectile geometries for both standard and custom designed bullets are tabulated in table 1. A standard 0.22 caliber bullet (Cascade Cartridges, Inc (CCI) Model #0032) was used as a comparison case and the same bullet type casing was used for reloading the unique designs.

In order to pack the custom bullets into a standard 0.22 caliber casing, the foot of the bullet was designed with a tight tolerance to allow for accurate press-fit into the casing (i.d. = 0.204 in, see figure 5). A press fit is necessary to ensure the maximum pressure behind the bullet is transferred to the bullet, thus resulting in maximum projectile velocity. If the fit is too tight then the bullets will require more pressure than available to eject from the casing and will not fire properly. To pack the custom bullets in the casing, a standard bullet was separated from the casing using a pair of pliers and a plate with a hole large enough to accommodate the casing and primer rim. After the standard bullet was removed, the casing was placed into a hole in a large steel block that is large enough to hold the modified bullet above the casing and ensure perfect alignment. Using a mallet and bronze shaft the modified bullet was press fit into the casing. In general, reloading 0.22 caliber rim fire rounds is not common, nor recommended by the manufacturer, and is potentially dangerous.

Directly above the foot of each bullet is the shoulder. The shoulder is the largest diameter of the entire bullet. As the bullet

4

Table 1. Designation of bullet types used in this study: # relates each bullet type to figure 6; *Material* explains the general make up of the bullet; ρ is the density of the bullet; *Model* indicates the bullet brand and model where indicated custom made bullets are indicated by MIT; *Shape* is a small schematic of the shape of the bullet; D_{tip} is the bullet tip size where ogive indicates a bullet tip that is defined by a continual curved surface at the tip; L/d_{tip} is the length to diameter ratio which was difficult to quantify for the standard bullets due to the curvature of the tip.

#	Material ρ [kg/m³]	Velocity [m/s] approx.	Model	Shape	D_{tip} [in] [in]	L/d_{tip}
1	Lead 11340	320	CCI/0032		ogive	~ 1.5
2	Lead 11340	370	CCI/0029		ogive	~ 1.5
3	Lead 11340	437	CCI/0047		Hollow	~ 1.5
4	Lead 11340	330	CCI/0027		ogive	~ 1.5
5	Lead 11340	720	CCI/0055		ogive	~ 1.5
6	Lead 11340	330	Eley/22LR		ogive	~ 1.5
7	Aluminum 2700	380	MIT Slug		0.22	7.2
8	Aluminum 2700	380	MIT Taper		0.15	10.5
9	Aluminum 2700	380	MIT Taper		0.12	13.9
10	Bronze 8300	380	MIT Slug		0.22	2.4
11	Bronze 8300	380	MIT Taper		0.15	3.7
12	Steel 7850	380	MIT Step		0.13	5.4
13	Aluminum 2700	440	MIT Step		0.06	29.5
14	Aluminum 2700	440	MIT Taper		0.06	29.5
15	Aluminum 2700	440	MIT Taper		0.06	29.5

passes through the barrel the shoulder engages with the rifling. This ensures that the pressure created after firing remains behind the bullet (not leaking past the sides of the bullet) pushing it through the barrel. If the bullet shoulder does not penetrate enough of the rifling then some of the explosive pressure from firing can leak past the bullet and reduce the back pressure, thus decreasing the velocity of the bullet down the barrel. It was assumed that the bullet exit velocities would be similar if the shoulders were identical diameters. However, this assumption did not hold in practice as some of the materials used for the modified bullets could not penetrate as much of the rifling since they were considerably harder than lead. Thus the modified bullets would often travel at lower speeds than the standard bullets. Rifling inside the barrel also forced the bullet to rotate about its longitudinal axis, ensuring stability of the bullet in air through gyroscopic stabilization. It should be noted that the modified bullets did not have sufficient spin rates for gyroscopic stabilization over long distances, however, the 3 meter distance to the target was sufficiently short for air-flight stability in this study [13, 14].

Ultimately, to ensure successful water entry, the primary design parameter for the bullets was the tip shape (see Experimental Results). Once the tip shape was determined, the bullet could be further designed to fit within the desired weight constraint. The modified angled disc cavity model was used to determine the relevant cavity shape for each bullet design. The model uses the bullet tip diameter and forward speed to determine the underwater cavity size. The remaining bullet shape is then designed to fit within the cavity, and the length to diameter adjusted so the bullets all weighed the same.

The standard bullets were fired from a Harrington & Richardson® Stevens™ 0.22 cal and modified bullets fired from a Harrington & Richardson® Sportster™ SSI-022 single shot. Both barrel riflings had a turn ratio of 1/16 or one bullet rotation in sixteen inches of forward travel. The rifles were mounted on a custom gun mount attached to a Manfrotto 410 three-axis geared head on a tripod which allowed for precise alignment of the projectile path with respect to the tank. The setup could easily be adjusted to half a degree increments along all three axis. A laser site was used to determine the point of impact of the projectile and a digital level was used to determine the angle of the gun in relation to the free surface.

Image acquisition and data processing

Each experiment was filmed by up to four high resolution high-speed cameras. As with all image capture techniques lighting and event timing were crucial elements linked to success. Images were then digitally processed to gather data to compare to models and to measure position and cavity shape. Four separate high-speed digital video cameras were positioned to allow visualization from multiple view points. The specifics of each camera and where they were positioned relative to the tank are

Table 2. The four cameras used in this study and their respective abilities.

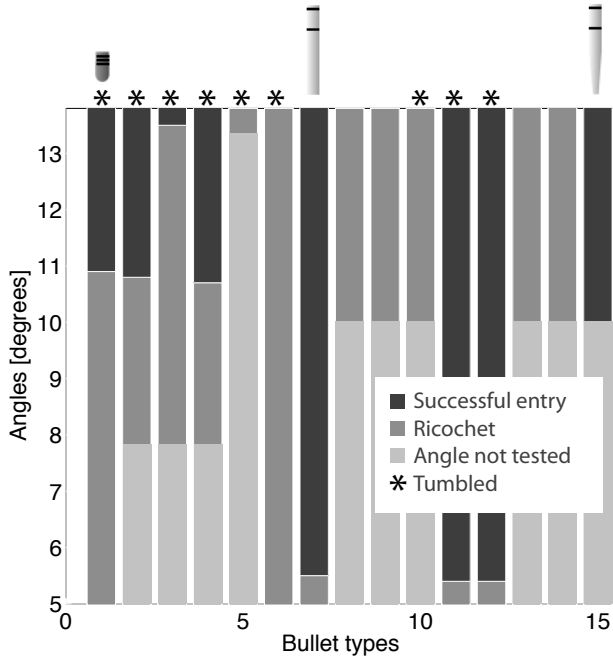| #	Name	Resolution	Frames per second [fps]	Maximum # images	Viewpoint
A	Shimadzu HyperVision HPV-1	312×260	1,000,000	103	Side
B	Phantom 7.3	512×256	25,000	8,000	Top
C	IDT X-Stream VISION XS-3	1280×460	2,300	6,000	Up-range
D	Photron Fastcam S A1	768×768	10,000	8,000	Side

Figure 6. Bullet tendency to skip when shot at given angles to the surface. The angles shown here are the angle of the gun to the water surface (α, figure 4). Bullet types are given by numbers and correspond to bullet types in table 1. Colors and symbols are referenced in the legend. The three bullet types presented in more detail are marked by images above chart, from left, 0.22 standard caliber bullet (1), 0.22 aluminum (7), 0.06 tapered aluminum (15).

for cavity size and allowed the bullet to be seen within the cavities when the cavities were large enough. Additional foreground lighting was achieved by a 1000 Watt spotlight positioned off-axis pointing towards the far end of the tank. Each event was externally triggered by a down-range sound sensor.

Image processing was used to determine the position of the bullet and the cavity shape for each video sequence recorded. The data provided the bullet forward trajectory and angular motion as well as the time evolution of the cavity and splash geometry. Standard edge detection methods were used to determine the bullet position. The edge detection algorithm found all sharp gradients in the image, then the appropriate edges were mapped to the bullet outline, the cavity, and the splash.

The bullet was typically no larger than 9 pixels in diameter in these images. Although this makes data collection easier it makes it difficult to estimate the location of the bullets with sub-pixel accuracy. Furthermore, to get the true center of gravity of the bullets it must be assumed that the bullets were aligned in the image focal plane. In reality the bullets precessed around their axis of symmetry, which caused them to move in and out of plane (but remain in focus) reducing the accuracy of the measurements. However, a good estimate of their position and velocity was found using the leading edge of the bullet. The cavity and splash were easier to identify accurately due to the strong index of refraction outline which appeared in every image.

Though 99 successful impacts were captured during this study only three are presented here to show the evolution of the bullet design. Furthermore, the data from only two cameras (C and D table 2) is presented to show the typical time evolution of the bullet through the water column.

summarized in table 2; cameras will be referred to as camera A, B, C or D in the text corresponding to this table.

Lighting was critical for high-contrast images and included both back and front light sources. Back lighting was provided by an array of 36 separately ballasted, florescent bulbs (32 Watt) positioned horizontally behind the tank, with a diffuser between the tank and the light bank to provide even field lighting. The back-lighting was the major key to allowing the images to be processed

EXPERIMENTAL RESULTS

Overall discussion of the behavior of the projectiles studied is presented in this section. Specific attention is given to the minimum entry angle for each bullet type and whether or not the particular bullets tumbled after entry. High-speed video images and kinematic data are presented for three distinct cases for bullet type 1, a standard 0.22 projectile, type 7, a modified aluminum slug projectile, and type 15, a special tapered aluminum projectile designed using the theoretical model (see table 1 for specific
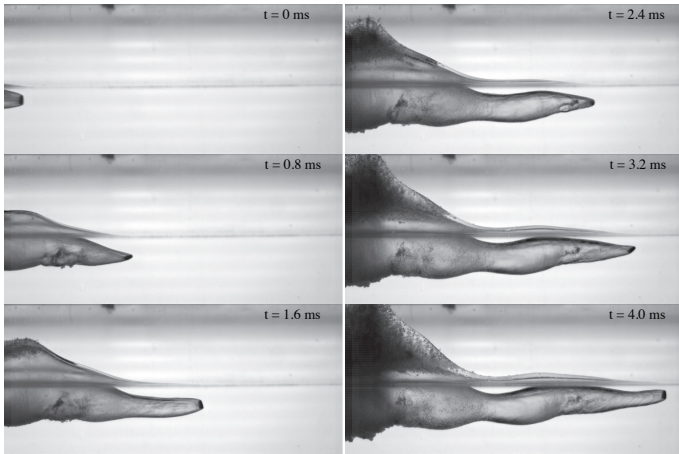
Figure 7. Images of a standard 0.22 caliber bullet case number 1. This bullet was fired at 380 m/s from the rifle barrel at an angle of 11° (table 1). The camera acquired images at 10000 fps, and every eighth image is shown here.
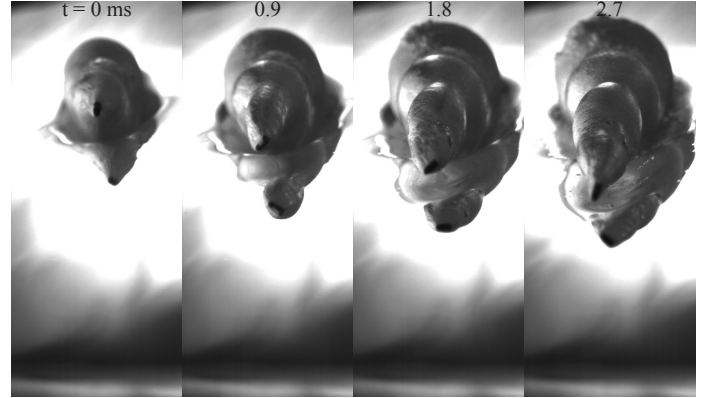

Figure 8. Images of a standard 0.22 caliber bullet case number 1 viewed looking at bullet head on (see figure 7 for speed and angle). The camera acquired images at 2260 fps, and every other image is presented here.

details of each bullet type). Comparisons of experimental results with the theoretical model formulation are also presented and discussed.

Ricochet and tumbling

Standard 0.22 bullet shapes have a tendency to skip out of the water when shot at shallow angles to the free surface. Like the standard 0.22 bullet, most shorter length-to-diameter bullets will almost always tumble if they enter the water, if they successfully break the free surface. In contrast, longer bullets with the same diameter have less of a tendency to tumble when traveling underwater but don't always enter the water successfully. Tests of 15 specific bullet types (see table 1) were performed over a range of entry angles from $5-15°$, and each set of data was analyzed to determine whether or not the bullets ricocheted off of the surface.

Figure 6 shows the relationship between the angle the bullets were shot at and their tendency to skip off of the surface for each of the 15 bullet types over a range of incidence angles: dark grey represents successful water entry for each type over a range of angles, grey represents cases that ricocheted, light grey areas were cases not tested due to time constraints or an obvious tendency to skip at low angles, and the asterisks at the top of each column indicate which cases tumbled after entry. Looking closely at the data, most standard bullets appear to enter successfully only when fired above 11°, whereas the custom 0.22 caliber aluminum bullet 7 can enter the water successfully down to angles of 5°. A few other bullet types did not skip at low angles down to 5° including case numbers 6, 7, 11 and 12, all of which are made of aluminum with large L/d_{tip} values and had varying

tip geometries. Note that bullet number 15 entered the water at angles above 10° but was not tested at lower angles due to limited access to the MIT Rifle Range.

Although the standard 0.22 caliber bullets did not skip off of the surface at angles above 11°, they did tumble inside their cavities almost immediately after impact; bullet types 10, 11, and 12 displayed similar tendencies to tumble. Tumbling of these cases is due in part to the short length to diameter ratio. The length of the aluminum slug (7) style bullet allows it to lean against the cavity as it begins to pitch or yaw, creating a planing force that directs the bullet back into the cavity before it can tumble. This reduces the velocity of the bullet due to drag, but allows it to maintain some stability as it passes through the water column. The larger the cavity is compared to the bullet diameter, the more likely the bullet is to have large pitching motion and thus more of a propensity to tumble. Cavity shape is dictated by the tip diameter as predicted by the theoretical model, thus a smaller tip should generate a narrower cavity and then enhance stability by allowing the back end of the bullet to ride on the cavity wall for support.

While many different bullets were tested and thousands of images were gathered, we only present three typical cases. First, the case when a standard bullet enters the water and tumbles until it either ejects out through the free surface, or tumbles to the bottom of the tank (e.g. figure 6, bullet type 1). Second, a successful water entry of a modified bullet with a large tip, which slows down rapidly and creates a cavity nearly four times larger than the aft portion of the projectile (e.g. figure 6, bullet type 7). Third, a modified bullet with a smaller tip that successfully enters the water and maintains a large velocity and kinetic energy after impact (e.g. figure 6, bullet type 15). Each of the cases 1, 7 and 15 are discussed in greater detail in the following sections and empirical results are compared with the theory presented above.
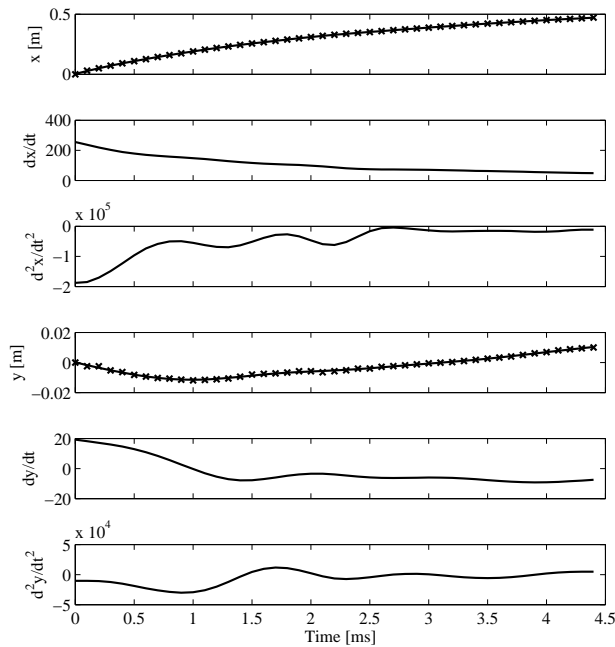
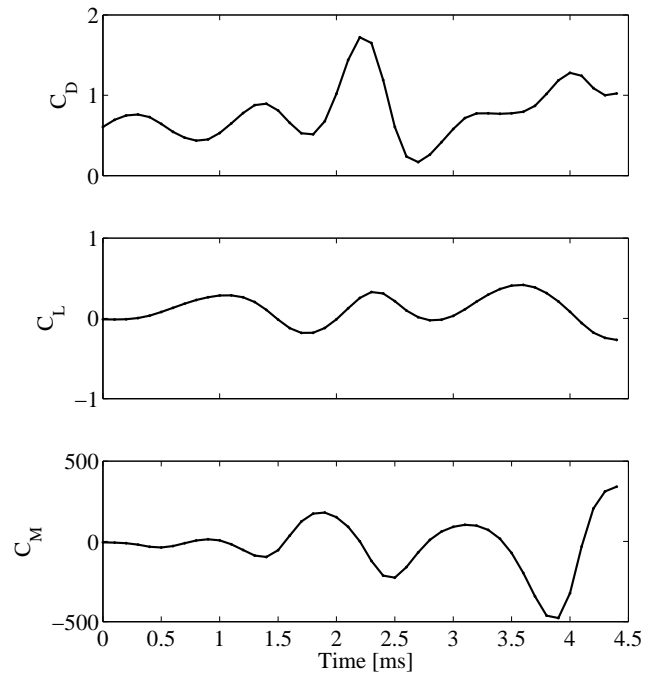Figure 9. Position, velocity, and accerlation in x and y for projectile impact shown in figure 7.

Figure 10. Coefficient of drag, lift, and moment for the projectile impact shown in figure 7.

Standard 0.22 projectile

Standard 0.22 bullet shapes have short length to diameter ratios and a rounded, ogive tip and are made from lead. They are not designed to be shot into the water, but are readily available and present a classic worst-case scenario for water entry. Figure 7 presents a time series of images for a standard 0.22 bullet entering the water at $11°$ and immediately beginning to tumble. At t = 0 ms (this time taken as the first frame in which the bullet is in the camera field of view) the projectile is already traveling with a $\theta = 90°$ angle of attack. As the projectile moves through the water it resides in a subsurface vapor cavity and tumbles uncontrollably.

Further evidence of tumbling can be seen in figure 8 in which the same bullet as figure 7 is viewed from head on. This particular image was obtained by placing a mirror in the tank which reflected the up-range image of the bullet coming downrange to camera C. In the figure the projectile appears in two places because the reflection off the underside of the quiescent free surface. The projectile not only tumbles, but it also appears to precess as the angle it makes with the horizon changes in time as well. This projectile is eventually ejected from the underwater cavity through the free surface due to its erratic behavior.

The kinematics of the bullet can be explored by looking at

the bullet velocity and acceleration as a function of time, both of which are derived from the x and y position data. Figure 9 shows the position, velocity and acceleration of the projectile in figures 7 & 8. The position data is approximated by finding the center of the bullet then applying a quintic spline to smooth the data (following the method presented in [15]); the smoothed spline is superimposed over the data points in figure 9 as a solid line.

The velocities of this projectile show the dramatic deceleration over this short distance: from 250 m/s to nearly 50 m/s in less than a meter. These large decelerations occur as a result of large energy lost to forming the cavity and increased drag due to tumbling. The accelerations reflect this as they show that the greatest decelerations occur at early times in x-direction but that decelerations in y fluctuate through flight and are an order of magnitude smaller than in the x-direction.

The forces associated with water entry are presented in figure 10. The magnitudes of the drag and lift forces are the product of the projectile mass and the projectile accelerations in x and y, resolved into local coordinates inline (drag) and normal (lift) to the bullet trajectory. All forces acting on the projectile, including viscous and added mass forces, are included in this formulation. Force coefficients for drag C_D and lift C_L are calculated by divid-
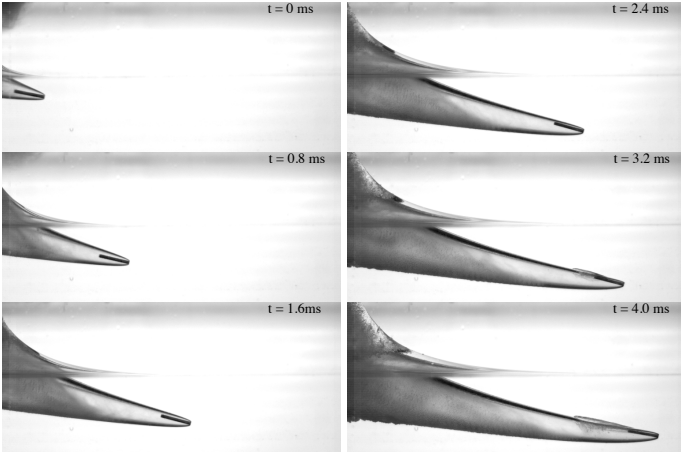
Copyright © 2009 by ASME

Figure 11. Time series of a modified 0.22 caliber aluminum bullet case number 7 (see figure 12 for speed and angle). Images are marked with a timestamp in the upper right hand corner indicating the time from the first image in the series. The darker patch in the upper left hand corner of t = 0 ms is a portion of the vaporous splash that is ejected upon impact. The camera acquired images at 10000 fps, and every eighth image is shown here.
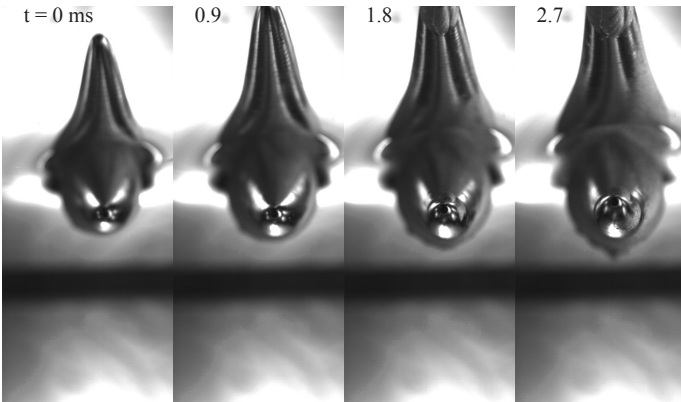

Figure 12. Images of a modified 0.22 caliber aluminum bullet case number 7 viewed looking at bullet head on. This bullet was fired at 380 m/s from the rifle barrel at an angle of 11° (table 1). The camera acquired images at 2260 fps, and every other image is presented here.

ing the forces by the product of the dynamic pressure $0.5\rho V_0^2$ and the frontal area of the projectile tip πR_0^2. The pitching moment is determined using the side view images and measuring the pitch angle as a function of time to find the rotational velocity of the bullet. The moment coefficient C_M is simply the product of the longitudinal moment of inertia of the projectile and the angular acceleration divided by the dynamic pressure, frontal area and length of the projectile.

In figure 10, the drag coefficient C_D oscillates slightly around a mean value of 0.5 and peaks when the bullet is transverse to the flow. The standard 0.22 caliber bullet has an $L/d_{tip} = 1.5$ and at any moment during its flight the frontal area of the tumbling projectile is between πR^2 (area of tip) or $6R^2$ (projected longitudinal area). Since force is normalized by the frontal area, the increase in C_D at the times when the bullet is transverse to the flow are expected. Looking at the videos the bullet is seen to both pitch and yaw inside the cavity and the overall cavity radius is affected by the tumbling behavior. The upstream images in figure 8 show the effect of the tumbling quite nicely in the bulbous nature of the cavity shape. As expected the average C_L is zero. The fluctuating component of C_L is approximately 180° out of phase with the moment coefficient C_M. The forces and moments fluctuate with an approximate frequency of 1000 Hz, revealing the unsteady nature of this type of water entry.

Modified aluminum 0.22 projectile

The behavior of the standard projectile can be greatly improved by altering the tip shape and increasing L/d_{tip}. Bullet type 7 is a slug-type model made from aluminum with a blunt leading edge, with no taper, and a long L/d_{tip}, compared to the standard 0.22.

The modified 0.22 slug was shot into the water at an angle of 11°. A time series of images shown in figure 11 reveals a clean cavity shape without the obvious oscillations seen in figure 7. The cavity is more uniform in shape and grows radially and in the direction of motion of the bullet. The projectile can be seen inside the cavity indicating that the cavity is quite large compared to the bullet diameter (approximately four times larger).

As the projectile passes through the water column the cavity grows, and a portion of the cavity splash is entrained into the cavity. The splash can be seen as a growing darker gray portion of the cavity on the left hand side of the images. As the projectile continues a downward descent it begins to pitch down such that the tail end eventually comes in contact with the upper portion of the cavity (t = 2.8 to 3.6 ms). The contact between the cavity and the tail of the projectile generates spray inside the cavity and deformation of the leading section of the cavity. The force of the projectile tail planing on the cavity wall forces the bullet to begin to pitch upwards (t = 4.0 to 4.8 ms *not shown*). This back and forth pitching motion continues until the bullet slows and the cavity collapses or the bullet hits the steel plate at the end of the tank.

Contact with the top of the cavity can be seen more closely in figure 12 in which the same projectile is viewed from head-on with the aid of an upstream mirror. At time t = 1.8 ms the projectile is already impacting the top of the cavity. The impact with the cavity can be seen most clearly by zooming into the mirrored reflection of the cavity onto the underside of the free surface (top of the image). The time steps in this image do not correspond to
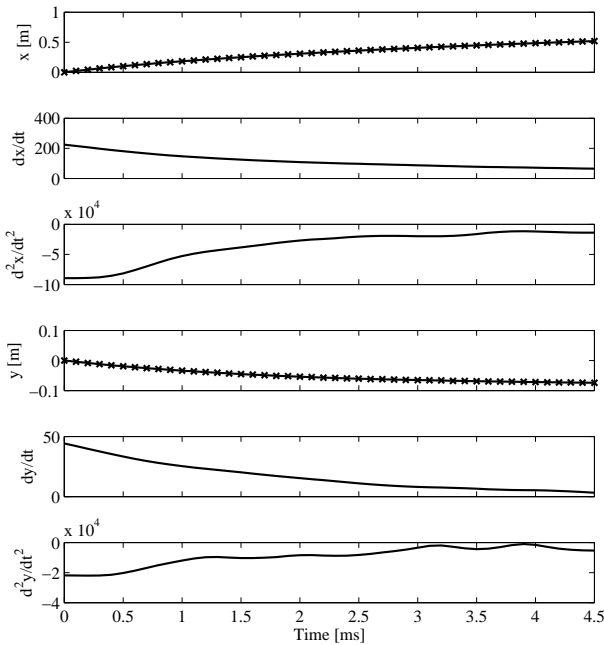
Copyright © 2009 by ASME

Figure 13. Position, velocity, and accerlation in x and y for projectile impact shown in figure 11.

Figure 14. Coefficient of drag, lift, and moment for the projectile impact shown in figure 11.

the same times as in figure 11 due to the arbitrary determination of t = 0 from when the bullet first appears in the images of any particular camera. Uniquely different camera types made timing extremely difficult and thus the images are not synchronized.

Looking at the velocities and accelerations it becomes apparent that the slug-type projectile is traveling in a much straighter path than that of the standard 0.22 bullet. Despite the straight trajectory and the clean cavity shape, figure 13 shows that the velocity in the x-direction follows an almost identical trend to that of the standard 0.22. This is likely due to the large frontal area of aluminum slug which is similar to that of the standard 0.22. The average drag coefficient for the bullet is $C_D = 0.5$ and C_D does not start to oscillate until the end of the run when the bullet is visibly pitching. The y-velocity is also similar to that of the standard 0.22 case, however, the magnitude of the unsteady oscillations in vertical acceleration appear smaller, presumably due the fact that the slug does not tumble.

Coefficients of drag, lift, and moment are presented in figure 14. The drag coefficient C_D shows a nearly constant value of 0.5 except for near the end of the run, as the projectile starts to pitch. The lift coefficient oscillates above zero as the back of the bullet skips along the top of the cavity wall (e.g. see figure 11 at 3.2 and 4.0 ms). The gradual change in the moment coefficient
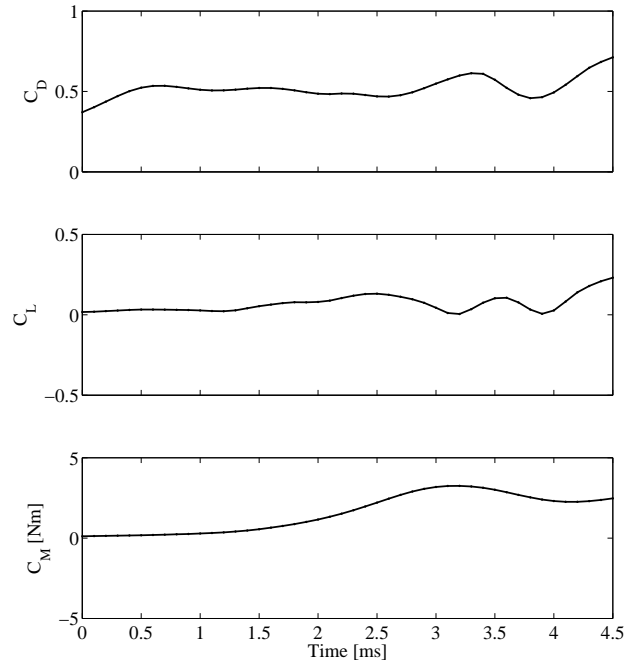
indicates a low pitching frequency and greater projectile stability inside the cavity. C_M peaks as the aft edge of the projectile touches the top of the cavity. After contact with the cavity wall the bullet begins to slowly pitch down again. Overall, the forces and moments reveal that this projectile is able to maintain generally stable and level flight, compared to the standard 0.22 bullet. The slug-type projectile also experiences high deceleration and a large overall cavity diameter compared to the bullet diameter. Ideally a smaller diameter cavity is necessary to improve performance and reduce deceleration rates. Therefore we turn to the theoretical model to design a better bullet.

Tapered aluminum 0.06 projectile

The two previously presented cases produce cavities nearly four times larger than the diameter of the bullets when measured near the foot. The straight and level flight achieved by the 0.22 caliber slug-type aluminum projectile could be improved if it generated a smaller cavity. The theoretical model predicts that smaller cavities are formed by smaller tip diameters. Furthermore, a smaller frontal area would result in reduced drag and overall reduced deceleration. Thus, a new bullet with a relatively smaller tip diameter (0.06 in.) compared to the aluminum slug was designed and tested. The theoretical model was used to de-
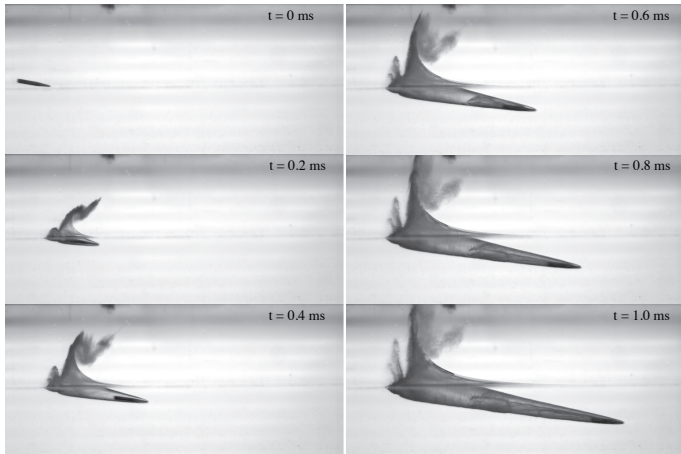
10

Figure 15. Time series of a modified 0.22 caliber aluminum bullet case number 15. This bullet was fired at 440 m/s from the rifle barrel at an angle of 11° (table 1). Images are marked with a timestamp in the upper right hand corner indicating the time from the first image in the series. The camera acquired images at 10000 fps, and every other image is shown here.
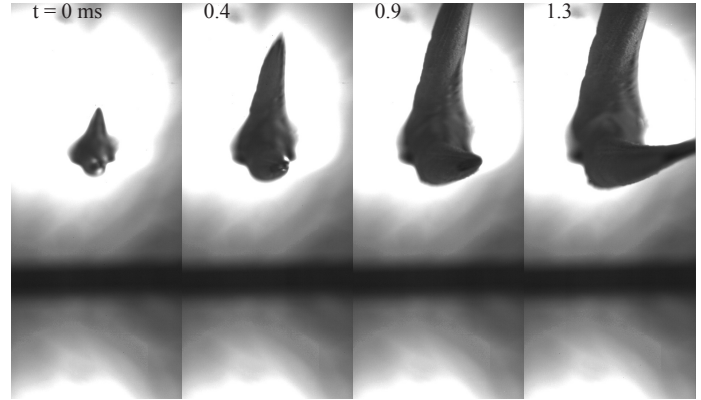

Figure 16. Images of a modified 0.22 caliber aluminum bullet case number 15 viewed looking at bullet head on (see figure 15 for speed and angle). The camera acquired images at 2260 fps, and every image in the series is presented here.

termine the aft-body shape of the bullet such that it would fit within the smaller cavity without touching the walls, when not pitching; the design resulted in a tapered projectile with a blunt tip.

The improved projectile behavior can be seen in figure 15. The cavity shape is greatly improved and the projectile fills much more of the cavity radially. At time $t = 0.4$ ms the size of the projectile inside the cavity can be seen most clearly. For this case $t = 0$ ms is taken before the bullet impacts the free-surface thus offsetting the time series data shown below. Entry speed is slightly higher than the previous two cases since the tapered bullet was packed into a different casing with more propulsive power (case 3 table 1). The projectile begins to lean against the cavity wall around $t = 0.5$ ms, appearing to kick up a spray inside the cavity. In an ideal case, the projectile would not lean against the cavity at all in an effort to keep the drag as low as possible and the trajectory straight. However, even planing on the cavity wall is preferable to tumbling. Through improved observations our understanding of how these projectiles behave when planing on curved cavities should lead to more efficient projectile designs and warrants further investigation.

Figure 16 shows a front view of the same projectile impact as in figure 15. Unfortunately, the projectile was aimed slightly off center and goes out of the field of view of the camera before too many details can be observed. This could indicate that this projectile does not oscillate inside the cavity but instead continually leans against the cavity wall. The image also reveals the much smaller cavity size. The short time span that the projectile

is in view is also an indicator of an increased velocity. The projectile goes on to break the mirror used to produce this shot just milliseconds after these images were taken (not shown). This is in contrast to the previously highlighted projectiles, which often impacted the mirror and bounced off, but did not break the mirror. That this projectile had enough kinetic energy to break through the mirror adds evidence of its decreased drag over the other cases.

The velocity and acceleration of this projectile are presented in figure 17. The projectile appears to hold a constant velocity for a short time before it begins to decelerate. As anticipated, the deceleration in x decreases but never really reaches the deceleration rate of case 7. Due to the high velocity of the projectile very few data points were collected before the bullet goes out of the field of view, in addition the bullets were often obscured from view inside the cavity making tracking difficult, and therefore increasing the error in the calculations of the derivatives for velocity and acceleration. It is also difficult to determine the location of the center of gravity for each projectile. Regardless, the data for the force and moment coefficients are presented in figure 18. It is good to note that this data is normalized by the tip area, thus for this tapered bullet the tip area is quite small compared to the slug-type and standard 0.22 bullets presented above.

The total drag on the bullet is the combination of the cavitator drag and the planing drag. The cavitator drag in the type 7 and type 15 bullets should be the same, the differences in drag coefficient being the planing drag nondimensionalized by different cavity diameters. Trends in C_D show a local maximum around 0.5 ms, when the back of the bullet first makes contact with the cavity wall. We expect that after its initial contact with the cavity the bullet pitches back into the cavity, reducing the drag force momentarily before it begins to decelerate at a greater rate, pre-
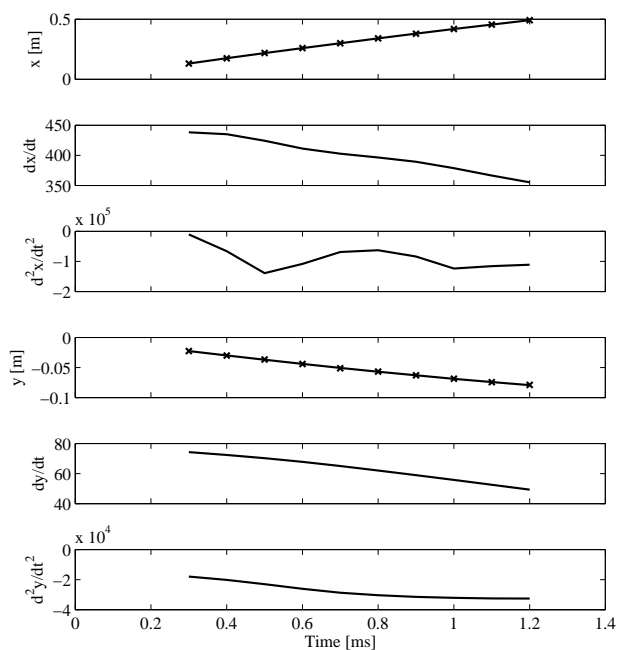
11

Figure 17. Position, velocity, and acceleration in x and y for projectile impact shown in figure 15.

Figure 18. Coefficient of drag, lift, and moment for the projectile impact shown in figure 15.

sumably due to the additional drag of the projectile planing on the cavity wall. C_M is relatively small, compared to the standard 0.22, and is constant throughout the run indicating that the projectile is most likely not being forced back into the cavity after making contact with the wall like we see in the slug-type case. We expect that contact with the cavity wall causes a momentarily increased drag as the projectile tail pushes through the cavity wall, but is then decreased as the projectile only skims along the surface of the cavity as it rides along inside.

DISCUSSION

The experimental data set presented herein represents the evolution of small caliber, high-speed, water-entry projectiles from standard bullet shapes to specially designed projectile types. As expected, we show that standard projectiles do not travel well underwater, yet modified blunt tip projectiles with large L/d_{tip} make axially uniform cavities and travel well inside of them. The performance of these projectiles is greatly improved by decreasing the tip size and adapting the overall shape to fit inside the cavities they form. The design is based on a well formulated theoretical model which predicts cavity shapes nicely.
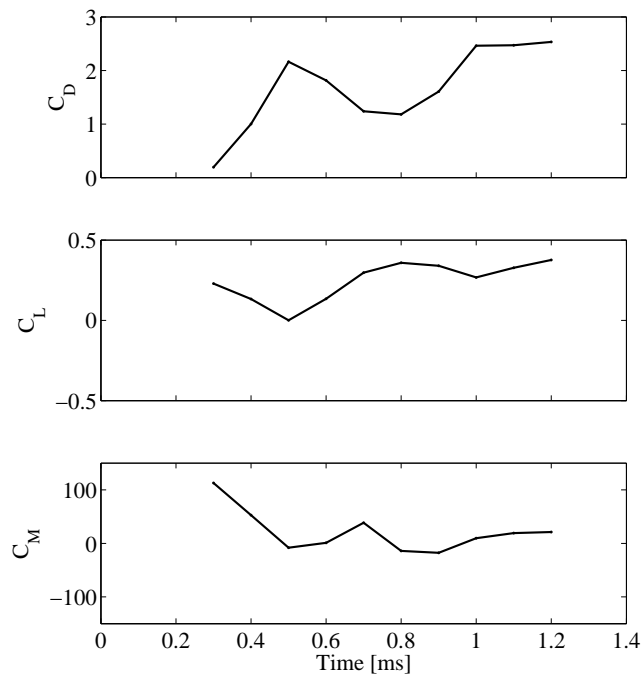
The experimental data shows the evolution of small caliber high-speed projectile water-entry from standard off-the-shelf bullet shapes to specifically designed underwater projectiles. Modified projectiles with blunt tips and large L/d_{tip} perform significantly better than the ogive tip small L/d_{tip} counterparts. The design is greatly enhanced through the application of a modified cavity model which accounts for small pitch angles. Using the cavity theory, better performing projectiles were designed and tested and experimental results show that the model is an accurate representation of the cavities observed.

Comparing the theoretical model presented herein to the empirical results found by tracing the cavities using an edge detection algorithm for cases 7 and 15, we find good overall agreement (see figure 19). Results show that our method of tilting the images and accounting for the angle of attack appear to yield comparable results except where the cavity is in contact with the free surface, as one might expect. Overall agreement emphasizes the usefulness in using the theoretical model when designing projectiles for optimum underwater flight.

This experimental study tested multiple bullet geometries to determine the validity of a commonly used cavity model developed by Logvinovich [1]. In so doing, the accuracy of the model was improved by updating its formulation and adding an angle

12
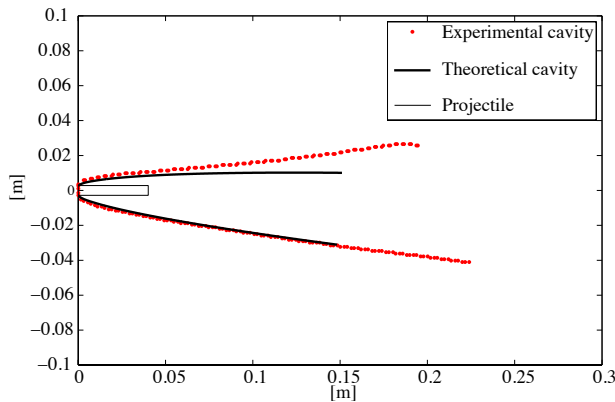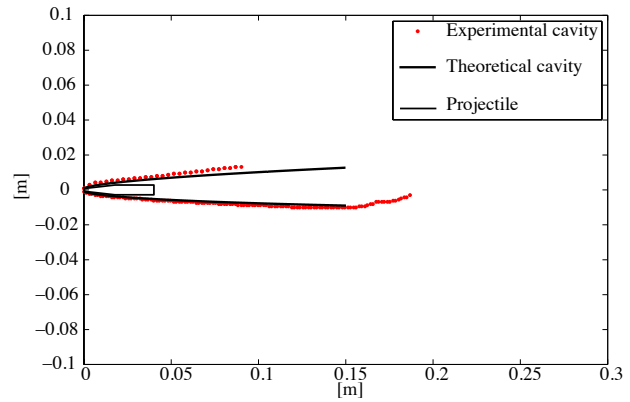
Figure 19. Modified Logvinovich angled disc compared to cavity from (a) case 7 and (b) case 15. (a) Experimental cavity obtained from images in figure 11, time = 1.2 ms, angle of attack is 4°, Velocity is 144 m/s and (b) from images in figure 15, time = 0.5 ms, angle of attack is -1°, Velocity is 430 m/s. Every fifth data point is plotted from the experiment in (···), and the cavity model is in black. For ease in processing these images are flipped horizontally from those in figure 11.

of attack correction. Despite the unsteady nature of this problem this improved steady state model fits well with experimental data. The data conclusively shows that bullets with lower length-to-diameter ratios tumble inside the vapor cavity, while higher length-to-diameter ratios can lean against the cavity walls inducing a planing force pushing them back inside the cavity mitigating the tumbling behavior. While the data presented herein are specific to 0.22 caliber bullets, findings can be readily extended to higher speed and higher caliber projectiles.

ACKNOWLEDGMENT

REFERENCES

[1] Logvinovich, G. V., 1972. *Hydrodynamics of free-boundary flows*. Jerusalem, Israel Program for Scientific Translation; [available from the U.S. Dept. of Commerce, National Technical Information Service, Springfield, Va.].

[2] Goeller, J. E., and Steves, H. K., 1999. Ramics projectile study. Tech. rep., Advanced Technology and research corporation (APR).

[3] Hrubes, J. D., 2001. "High-speed imaging of supercavitating underwater projectiles". *Experiments in Fluids,* **30**(1), pp. 57 – 64.

[4] May, A., 1952. "Vertical entry of missiles into water". *Journal of Applied Physics,* **23**(12), pp. 1362–1372.

[5] Gilbarg, D., and Anderson, R. A., 1948. "Influence of atmospheric pressure on the phenomena accompanying the entry of spheres into water". *Journal of Applied Physics,* **19**(2), pp. 127–139.

[6] Shi, H.-H., Itoh, M., and Takami, T., 2000. "Optical observation of the supercavitation induced by high-speed water entry". *Journal of Fluids Engineering,* **122**(4), pp. 806–810.

[7] Paryshev, E. V., 2006. "Approximate mathematical models in high speed hydrodynamics". *Journal of Engineering Mathematics,* **55**, pp. 41–64.

[8] Savchenko, Y., Semenenko, V., Putilin, S., Savchenko, V., and Naumova, Y., 2000. Theory of stable model motion with ventilated and unventilated supercavities. Review, National Academy of Sciences of Ukraine Instittue of Hydromechanics Department of Free Boundary Flows, Kyiv.

[9] Grady, R. J., 1979. *Hydroballistics design handbook Volume 1*. Naval Sea Systems command Hydromechanics Committee, January.

[10] May, A., and Hoover, W. R., 1963. A study of the water-

entry cavity. Unclassified NOLTR 63-264, United States Naval Ordinance Laboratory, White Oak, Maryland.

[11] May, A., 1975. Water entry and the cavity-running behavior of missiles. Tech. Rep. 20910, Naval Surface Weapons Center White Oak Laboratory.

[12] Neaves, M. D., and Edwards, J. R., 2006. "All-speed time-accurate underwater projectile calculations using a preconditioning algorithm". *ASME,* **128**, March, pp. 284–296.

[13] Truscott, T. T., 2009. "Cavity dynamics of water entry for spheres and ballistic projectiles". PhD thesis, Massachusetts Institute of Technology.

[14] McCoy, R. L., 1999. *Modern Exterior Ballistics*. Schiffer Publishing Ltd., 4880 Lower Valley Road, Atglen, PA 19310.

[15] Epps, B. P., Truscott, T. T., and Techet, A. H., 2009. "A robust method for curve fitting and evaluating derivatives of experimental data using smoothing splines". *In Prep.*